

Structure of the ^{11}Li continuum from breakup on proton target

S. N. Ershov

Joint Institute for Nuclear Research, 141980 Dubna, Russia

B. V. Danilin

Russian Research Center "The Kurchatov Institute," 123182 Moscow, Russia

J. S. Vaagen

SENTEF Department of Physics, University of Bergen, Bergen, Norway

A. A. Korshennikov*

RIKEN, Wako, Saitama 351-0198, Japan

I. J. Thompson

Department of Physics, University of Surrey, Guildford GU2 7XH, United Kingdom

(Received 18 March 2004; published 15 November 2004)

Inelastic scattering of ^{11}Li on proton targets at energy of 68 MeV/nucleon has been studied in the microscopic four-body distorted-wave model. The ground state and three-body continuum excitations of ^{11}Li were calculated in the $^9\text{Li}+n+n$ cluster model using the method of hyperspherical harmonics. The theory describes the experimental data well and clarifies contributions from the three-body monopole resonance in ^{11}Li and from its soft dipole excitation. Various aspects of the ^{11}Li excitations and their nature are discussed in terms of correlation plots.

DOI: 10.1103/PhysRevC.70.054608

PACS number(s): 24.30.Gd, 24.10.Ht, 25.40.Cm, 27.20.+n

I. INTRODUCTION

Two-neutron halos have by now been found in many light dripline nuclei, in the cardinal cases ^6He and ^{11}Li , but also in ^{14}Be , ^{17}B , and carbon and oxygen isotopes. In Borromean halo nuclei the three-body continuum is most intriguing. For example, in the case of ^6He , a concentration of transition strengths is experimentally observed at 1–3 MeV above the $\alpha+n+n$ threshold in addition to the well known 2^+ resonance, and the nature of this strength is still being clarified. A similar situation pertains to the case of ^{11}Li , where a peak is experimentally observed at ~ 1 MeV above the $^9\text{Li}+n+n$ threshold. These strength concentrations may contain ordinary resonances or a new kind of collective motion, a soft dipole mode of excitation corresponding to oscillations of the core against the halo neutrons. It is still an open question whether the soft dipole excitations can be related to a pole in the S matrix.

The intrinsic properties of the continuum of Borromean nuclei could in principle be revealed in $3 \rightarrow 3$ scattering. To perform such an experiment is, however, practically impossible. Thus we have to resort to binary reactions, where the continuum is usually explored via responses which are induced by transitions from the ground state to the continuum. A reliable way to study the continuum properties is to explore nuclear reactions under conditions where one-step transitions dominate. This is, however, still a rather comprehen-

sive task, because of the intertwining of the ground state and continuum structures, influenced by reaction mechanisms.

Breakup reactions with fast beams of exotic nuclei are a powerful tool for investigations of halo nuclei. In the present paper we consider ^{11}Li breakup on a proton target at energy $E/A=68$ MeV. This reaction has been experimentally studied in Ref. [1] by correlation measurements of the emitted particles. Only one previous microscopic calculation of the ^{11}Li inelastic scattering has been attempted [2], with analysis of the excitation spectrum from Ref. [1], using a multiple scattering expansion of the total transition amplitude. In the present paper we probe the ^{11}Li inelastic scattering using the four-body distorted-wave reaction model [3–6] which allows calculations of all observables in processes leading to low-energy excitations of Borromean two-neutron halo nuclei. A three-body model of ^{11}Li , the same as that of Ref. [2], is used in the microscopic calculations. The calculations are compared with available experimental data on the elastic and inelastic scattering. Extracted three-body monopole and dipole excitations in ^{11}Li are discussed in detail.

II. THEORETICAL FORMALISM FOR HALO EXCITATIONS**A. Breakup reaction mechanism**

The prior form of an exact transition matrix T_{fi} for ^{11}Li breakup into two halo neutrons and a ^9Li core, in collision with a proton target, is given (for details see Refs. [3–6]) by

*On leave from the Russian Research Center "The Kurchatov Institute," 123182 Moscow, Russia.

$$T_{fi} = \left\langle \Psi_{m_b, m_1, m_2, m_C}^{(-)}(\mathbf{k}_x, \mathbf{k}_y, \mathbf{k}_f) \left| \sum_j V_{pj} - U_{^{11}\text{Li}} \right| \psi_{J_i M_i} \chi_{i, m_a}^{(+)}(\mathbf{k}_i) \right\rangle. \quad (1)$$

Here $\Psi_{m_b, m_1, m_2, m_C}^{(-)}$ is the full scattering solution with ingoing wave boundary condition, m_b , m_1 , m_2 , and m_C being spin projections of the proton target, halo neutrons, and ^9Li core (C), respectively. $\psi_{J_i M_i}$ is the ground state wave function of ^{11}Li . The distorted wave $\chi_{i, m_a}^{(+)}$ describes the proton- ^{11}Li relative motion in the initial channel and is a solution of the Schrödinger equation with optical potential $U_{^{11}\text{Li}}$. The proton-nucleon interaction V_{pj} is summed over all nucleons j in ^{11}Li . Due to Galilean invariance only relative momenta \mathbf{k}_x , \mathbf{k}_y , and $\mathbf{k}_{i,f}$ can characterize the reaction dynamics. These are, respectively, the relative momenta within a pair of fragments, between the center mass of the pair and the third fragment, and between the center of mass of the halo nucleus and target in the initial and final channels. In the halo nucleus rest frame, \mathbf{k}_y corresponds to the momentum of the third fragment. We know that recoil effects, due to translational invariance, are very important in light nuclei. In halo nuclei a correct treatment of translational invariance is even more significant due to the extremely large spatial extension of these systems.

The exact T matrix (1) cannot be calculated without approximations. The character of the approximations is defined by reaction conditions. At large momentum between two fragments it is possible to neglect the interaction between them. However, if the halo nucleus is excited to low energies E_κ above the three-body threshold ($E_\kappa = \varepsilon_x + \varepsilon_y = k_x^2/2\mu_x + k_y^2/2\mu_y$, where $\mu_{x,y}$ are reduced masses; the core C is in its ground state), the momenta $k_{x,y}$ are both small. Then there is no physical reason to neglect any pairwise interaction between the fragments. There are no spectators; all fragments are participants. It is important to observe that the low-energy region of nuclear excitations is most sensitive to the halo structure.

At high enough collision energy, when one-step processes dominate, a simplified treatment is possible for the reaction mechanisms leading to low-energy halo excitations. In such conditions the distorted-wave treatment of the reaction dynamics can be used and the scattering wave function $\Psi_{m_b, m_1, m_2, m_C}^{(-)}(\mathbf{k}_x, \mathbf{k}_y, \mathbf{k}_f)$ can be written as a product, giving an approximate transition matrix

$$T_{fi} = \left\langle \chi_{f, m_b}^{(-)}(\mathbf{k}_f) \psi_{m_1, m_2, m_C}^{(-)}(\mathbf{k}_x, \mathbf{k}_y) \left| \sum_j V_{pj} \right| \psi_{J_i M_i} \chi_{i, m_a}^{(+)}(\mathbf{k}_i) \right\rangle. \quad (2)$$

Here $\chi_{f, m_b}^{(-)}(\mathbf{k}_f)$ is a distorted wave describing proton-ejectile relative motion in the final channel, while $\psi_{m_1, m_2, m_C}^{(-)}(\mathbf{k}_x, \mathbf{k}_y)$ is a three-body ($^9\text{Li} + n + n$) continuum wave function. In calculations of $\psi_{m_1, m_2, m_C}^{(-)}(\mathbf{k}_x, \mathbf{k}_y)$ all pairwise interactions between fragments must be taken into account or, in other words, full scale final state interactions must be included. The term in Eq. (1) which contains the optical potential $U_{^{11}\text{Li}}$ does not give a contribution in Eq. (2) due to orthogonality between

the ground state $\psi_{J_i M_i}$ and the continuum $\psi_{m_1, m_2, m_C}^{(-)}(\mathbf{k}_x, \mathbf{k}_y)$ wave functions. The reaction model based on the approximation (2) has been successfully applied [3–7] to reactions with ^6He projectiles.

Expression (2) shows that the reaction amplitude is defined by three ingredients: (i) the nuclear structure contained in transition densities from the ground state $\psi_{J_i M_i}$ to the continuum $\psi_{m_1, m_2, m_C}^{(-)}(\mathbf{k}_x, \mathbf{k}_y)$ states; (ii) the effective interactions V_{pj} between the projectile and target nucleons; (iii) the distorted waves $\chi_{i, m_a}^{(+)}$ describing relative motion of the colliding systems. At present it is out of reach to treat all ingredients, nuclear structure and reaction dynamics, within a unified approach based on the same interactions, and one has to use different effective forces for description of nuclear structure and reaction mechanisms. The ingredients (ii) and (iii) can however be connected since properties of the effective nucleon-nucleon interaction are manifested in the nucleon-nucleus scattering potentials. Self-consistency requires that the effective interaction V_{pj} , which is responsible for the reaction, is also used for calculation of optical potentials necessary for the distorted-wave calculations. Thus experimental data on elastic scattering and total reaction cross sections can be used to define the effective interaction V_{pj} and check the accuracy of calculations of the distorted wave functions. This procedure limits strongly the freedom of V_{pj} modifications in breakup reaction calculations. We also note that the interactions with all (core and halo) nucleons in the projectile are added coherently in the reaction amplitude (2). Thus the interplay between the core and halo degrees of freedom becomes essential, and has a strong impact on reaction dynamics.

B. Model for the ^{11}Li nucleus

The interaction cross section of high-energy beams of Borromean halo nuclei with light targets has been proven to be approximately equal to the sum of the separate interaction cross section of the core nucleus and the two-neutron removal cross section [8]. This indicates that the reaction process affects the core and halo subsystems separately, and underpins the very halo concept, i.e., that the wave function $|\psi\rangle$ of a halo nucleus may be approximated by a product

$$|\psi\rangle = |\varphi_{\text{core}}\rangle |\psi_{\text{halo}}\rangle,$$

where $|\varphi_{\text{core}}\rangle$ corresponds to the internal structure of the core and $|\psi_{\text{halo}}\rangle$ describes the relative three-body motion of the halo neutrons and the core [9–11]. Within this model, extended with an approximate treatment of the Pauli principle, it is possible to give a consistent description of main properties of both the ground state and the low-energy continuum wave functions of Borromean halo nuclei. The method of hyperspherical harmonics was used for calculating the ground and continuum three-body wave functions. Detailed description of the formalism can be found in [10,11]. Since the reactions involve transition properties of the halo nucleus, transition densities [3,6] from the ground state to the continuum under the influence of point perturbations have been calculated. This model implies separate transition den-

sities corresponding to nuclear responses from the halo and core nucleons.

For the n - n interaction between halo neutrons we used the soft core realistic GPT potential [12], containing central, spin-orbit, and tensor forces. The parameters of the n -core potential correspond to the (P2) model of the ^{11}Li ground and continuum states [2,13]. This potential includes (i) a central part of Woods-Saxon type with parameters $r_0=1.27$ fm, $a=0.67$ fm, and $V_0=-50.45$ MeV and -39.1 MeV for s and p, d waves, respectively; (ii) a spin-orbit potential of a derivative of a Woods-Saxon form factor with $V_{ls}=8.94$ MeV. All partial components of the n -core potential with $l>2$ were omitted. The Pauli projection method was employed to eliminate the Pauli forbidden $0s_{1/2}$ and $0p_{3/2}$ states in the n - ^9Li subsystem in the three-body calculations and the spin of the ^9Li core was ignored. The ^9Li density was described by a Gaussian distribution with a range parameter chosen to reproduce the empirical matter radius of ^9Li , $\langle r^2 \rangle^{1/2}=2.32$ fm.

Hypermoments up to $K_{\max}=20$ were included for 0^+ (ground state and continuum) and $K_{\max}=19$ for 1^- excitations. For the ground state the calculation gives a binding energy 0.242 MeV, matter radius $\langle r^2 \rangle^{1/2}=3.32$ fm, and a superposition of the $(0p_{1/2})^2$ and $(1s_{1/2})^2$ components in the wave function with weights of 45% and 31%, respectively. This model describes data on the ^{11}Li matter radius, momentum distributions of fragments, and β decay [13].

The monopole 0^+ and dipole 1^- low-energy excitations in ^{11}Li were consistently calculated with the same input. As in Ref. [2], the calculations of monopole phase shifts revealed a possible three-body 0^+ resonance state near the threshold, formed as a superposition of s^2 and p^2 configurations and orthogonal to the ground state. The dipole continuum was found to have a pronounced peak in the excitation spectrum. Its phase shifts show at most a resonantlike structure; it is, however, not a "true" three-body resonance from phase shift criteria (see details in [2]).

Other low-energy transitions (quadrupole 2^+ excitation as well as spin-flip 0^- and 1^+ excitations) should be very weak near threshold in the ^{11}Li inelastic scattering at the energy of 68 MeV/nucleon [2,14].

C. Effective forces and elastic scattering

The distorted waves $\chi_{i,f}^{(\pm)}$ for the breakup calculations were obtained by solving the Schrödinger equation with the microscopic optical potential $U_{^{11}\text{Li}}$. The optical potential was calculated in the single folding model and has two parts, U_{core} and U_{halo} , created by interactions of the proton target with the core nucleons and the halo neutrons, respectively,

$$\begin{aligned} U_{^{11}\text{Li}}(\mathbf{r}) &= U_{\text{core}}(\mathbf{r}) + U_{\text{halo}}(\mathbf{r}) \\ &= \int d\mathbf{r}' V_{NN}(\mathbf{r}-\mathbf{r}')\rho_{\text{core}}(\mathbf{r}') \\ &\quad + \int d\mathbf{r}' t_{NN}(\mathbf{r}-\mathbf{r}')\rho_{\text{halo}}(\mathbf{r}'), \end{aligned} \quad (3)$$

where ρ_{core} and ρ_{halo} are the ground state densities of the core nucleons and the halo neutrons.

The density $\rho_{\text{core}}(\mathbf{r})$ is determined by a convolution integral of the ^9Li density $\rho_{^9\text{Li}}(\mathbf{r})$ and the density $\rho_{\text{c.m.}}(\mathbf{r})$ describing a motion of center of mass of the core. In momentum space, this relation has the product form $\rho_{\text{core}}(\mathbf{q}) = \rho_{^9\text{Li}}(\mathbf{q})\rho_{\text{c.m.}}(\mathbf{q})$. Thus simultaneously with $U_{^{11}\text{Li}}$ we can calculate an optical potential for ^9Li -proton scattering,

$$U_{^9\text{Li}}(\mathbf{r}) = \int d\mathbf{r}' V_{NN}(\mathbf{r}-\mathbf{r}')\rho_{^9\text{Li}}(\mathbf{r}'). \quad (4)$$

The Jeukenne-Lejeune-Mahaux (JLM) forces [15] in the improved local density approximation, with normalization factor $\lambda=0.8$ for the real and imaginary parts, were used for interactions ($V_{pj} \equiv V_{NN}$) with the core nucleons. This complex interaction is based on the Brueckner-Hartree-Fock approximation and is both energy and density dependent and has successfully been applied for optical potential calculations in stable nuclei. Since the JLM interaction has a central part only, the spin-orbit components of the M3Y forces [16] was added to produce a spin-orbit part of the optical potential coming from interaction with the core. Such a combination of central (JLM) and spin-orbit (M3Y) effective interactions provides a good description of nucleon-nucleus scattering data on $^{6,7}\text{Li}$ [17].

Since the halo neutrons are most of the time outside the core region, their interaction with the proton target must be similar to interaction of free nucleons. Thus the free NN t matrix forces [18] were used for the proton target interactions with the halo neutrons ($V_{pj} \equiv t_{NN}$). This complex, energy dependent interaction describes free nucleon-nucleon scattering and accounts for an infinite number of NN rescatterings.

Figure 1 shows (solid lines) the real and imaginary parts of the ^{11}Li optical potential for the collision energy of 68 MeV/nucleon. The dashed and dotted lines show contributions to the potential from the core (U_{core}) and halo (U_{halo}) nucleons, respectively. We observe that the contributions from the halo have long range character, as expected, and dominate the potential at large radii. The real and imaginary halo potentials have (for a rather wide range of beam energies) somewhat different shapes but comparable absolute values. The picture is different for the core potential, where the real part is a few times larger than the imaginary one. As a result, interactions with the halo neutrons give a significant modification of the imaginary part of the optical potential, but only minor influence on the real part.

Figure 2 shows comparison of theoretical angular distributions for the elastic scattering of both ^{11}Li and ^9Li with experimental data [1,19]. A quite reasonable description of the ^9Li elastic data in the angular region $\theta \leq 40^\circ$ is obtained, given that our knowledge of the ^9Li density distribution is rather poor (only gross geometry, the rms radius, was fixed). We do not consider it meaningful to play with the effective forces to improve agreement at larger angles. For ^{11}Li the precise shape of the core is somewhat less important due to smoothing effects from the ^9Li center of mass motion. For ^{11}Li the theoretical calculation describes both shape and ab-

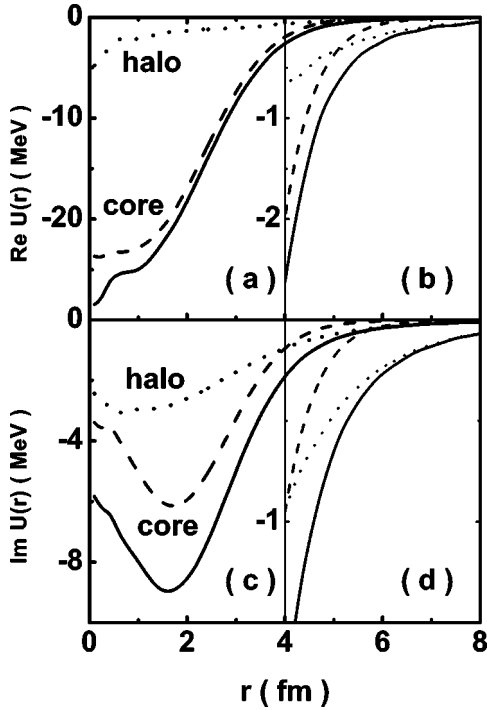


FIG. 1. The microscopic optical potential for $^{11}\text{Li}+p$ scattering at $E/A=68$ MeV. (a) Real part. (c) Imaginary part. (b) and (d) show the tails of the real and imaginary parts of the potentials. Solid, dashed, and dotted lines correspond to the total potential and contributions from the core and halo nucleons, respectively.

solute value of the elastic angular distribution quite well.

It is of interest to understand in detail what dynamical features of the model are responsible for a correct reproduction of the difference in the character of ^{11}Li elastic scattering compared with the scattering of ^9Li . Dotted and dashed

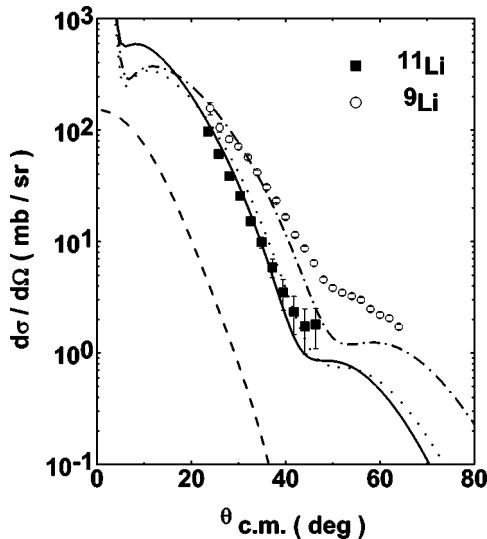


FIG. 2. Angular distributions for calculated elastic scattering of ^{11}Li and ^9Li on a proton target compared with experiment [1,19]. Solid and dash-dotted lines show results for ^{11}Li and ^9Li . Dashed and dotted lines show contributions to the elastic scattering of ^{11}Li from the halo neutrons and the core nucleons, respectively.

lines in Fig. 2 show the theoretical fictitious elastic scattering due to two separate parts of the optical potential in Eq. (3), U_{core} and U_{halo} , created by interactions with the core nucleons and the halo neutrons, respectively. The elastic scattering from the core nucleons dominates at all angles. This conclusion was also obtained in Ref. [20]. The scattering on the halo neutrons is important only in the forward direction ($\theta \leq 20^\circ$) producing a constructive interference with the core contribution. Owing to the core center of mass motion, the space occupied by the ^9Li core when embedded in ^{11}Li is effectively larger than when ^9Li is free. Thus the slope of the angular distribution from a moving core (dotted line) is steeper than from a free core (dash-dotted line).

The role of the halo neutrons is, however, amplified if we study reaction cross sections. The calculated reaction cross section for ^{11}Li (398 mb) is significantly larger than for ^9Li (234 mb). The contributions to the reaction cross section from the halo neutrons (U_{halo}) and nine core nucleons (U_{core}) are about the same, 231 and 226 mb, respectively. This strong influence on absorption properties reflects the fragile nature of the halo neutrons which are easily kicked out whenever hit by the proton.

Finally, in the case of inelastic scattering calculations, the full implementation of the two-body spin-orbit forces would require calculations of the current and spin-current transition densities [3]. It demands a precise knowledge of the spin and velocity dependence of the effective interactions in ^{11}Li , a knowledge which so far is not available, and a better treatment of spin structure of ^{11}Li . At small transferred momenta the current densities are, however, usually small; thus we neglected their contributions and, correspondingly, did not include spin-orbit forces in the breakup calculations.

D. Identification of a “true” three-body resonance

For two halo neutrons and core, two sets of Jacobi coordinates can be defined. In one of them, T , the x coordinate corresponds to the n - n subsystem while y refers to $(nn)-C$. In the second case, Y , the x and y denote n - C and $(nC)-n$, respectively. In both cases the Jacobi coordinates are related to the physical distances by appropriate mass scaling. The energy E_κ and the three-body phase space $\sqrt{\epsilon_x \epsilon_y} d\epsilon_x d\epsilon_y$ are invariant for any binary partitions [$E_\kappa = \epsilon_x + \epsilon_y = E_{nn} + E_{(nn)-C} = E_{Cn} + E_{(Cn)-n}$ and $k_x^2 dk_x k_y^2 dk_y = 2(\mu_x \mu_y)^{3/2} \sqrt{\epsilon_x \epsilon_y} d\epsilon_x d\epsilon_y$].

In order to have a reference case where analytical estimates are possible, we have used the following approximation. Using the hyperharmonics method and taking into account the close analogy between partial wave expansions in the two-body and three-body problems, we consider, in first approximation, the diagonal parts of the continuum wave function. Then (for given J^π) the resonant three-body wave function takes, in the interior region, the form given in Refs. [21,22] (neutron spins are not indicated explicitly):

$$\psi(\rho \Omega_5^p, E_\kappa \Omega_5^\kappa) \propto \frac{1}{(\kappa \rho)^{5/2}} \sum_{K,\gamma} C_{K\gamma}(E_\kappa) \psi_{K\gamma}^R(\rho) Y_{K\gamma}(\Omega_5^p) Y_{K\gamma}(\Omega_5^\kappa) \quad (5)$$

with

$$|C_{K\gamma}(E_\kappa)|^2 = \frac{\Gamma_{K\gamma}}{(E_\kappa - E_0)^2 + \Gamma^2/4}. \quad (6)$$

Here K is the hypermoment, $\gamma=(l_x, l_y, L)$ denotes the Jacobi orbital and total orbital angular momenta, $Y_{K\gamma}(\Omega_5)$ is the hyperspherical harmonic dependent on spatial Ω_5^K or momentum Ω_5^K angles in hyperspherical coordinates [10], E_0 is the position of the resonance, $\Gamma_{K\gamma}$ is the partial width, and Γ is the total width. $\psi_{K\gamma}^R(\rho)$ is the *energy-independent* form of the internal part of the resonant wave function. We see from Eq. (6) that the dependence of a three-body resonance on E_κ has a pole character typical for an ordinary Breit-Wigner resonance. In the case of a resonance near threshold, the component with minimal value of hypermoment K_0 dominates in the scattering wave function (5). Using this one-component (K_0) expression for the continuum wave function in the transition matrix (2) leads to a factorized expression for the inelastic scattering cross section. Integration over all angles of the $\mathbf{k}_x, \mathbf{k}_y$ momenta gives the double differential cross section:

$$\begin{aligned} \frac{d^2\sigma}{d\varepsilon_x d\varepsilon_y} &\propto (E_\kappa)^{-5/2} \sqrt{\varepsilon_x \varepsilon_y} \sum_\gamma |C_{K_0\gamma}(E_\kappa)|^2 |\psi_{K_0}^{l_x l_y}(\alpha_\kappa)|^2 \\ &= \frac{(E_\kappa)^{-5/2} \sqrt{\varepsilon_x \varepsilon_y} \sum_\gamma \Gamma_{K_0\gamma} |\psi_{K_0}^{l_x l_y}(\alpha_\kappa)|^2}{(\varepsilon_x + \varepsilon_y - E_0)^2 + \Gamma^2/4}, \end{aligned} \quad (7)$$

where $\psi_{K_0}^{l_x l_y}(\alpha_\kappa)$ is the hyperangular part of the hyperharmonics [10], $\sin^2 \alpha_\kappa = \varepsilon_x / E_\kappa$. Near threshold and in the case of not so narrow resonance $\Gamma \sim E_0$, the energy dependence of widths $\Gamma_{K_0\gamma}$ and Γ has to be taken into account. In the simplest approximation, the three-body width is proportional to the three-body phase volume, $\Gamma_{K_0\gamma} \propto E_\kappa^2$. For the state J^π with lowest K_0 we obtain the form

$$\begin{aligned} \frac{d^2\sigma}{d\varepsilon_x d\varepsilon_y} &\propto \frac{\sqrt{\varepsilon_x \varepsilon_y} (\varepsilon_x + \varepsilon_y)^{-1/2}}{(\varepsilon_x + \varepsilon_y - E_0)^2 + \Gamma_0^2 (E_\kappa / E_0)^4 / 4} \\ &\quad \times \sum_{l_x, l_y} (\varepsilon_x / E_\kappa)^{l_x} (\varepsilon_y / E_\kappa)^{l_y} \end{aligned} \quad (8)$$

where a simple parametrization of energy dependence is used for the total width $\Gamma = \Gamma_0 (E_\kappa / E_0)^2$. Integration of Eq. (8) over the hyperangle α_κ gives an asymmetric resonance shape for the three-body decaying state:

$$\frac{d\sigma}{dE_\kappa} \propto \frac{E_\kappa^{3/2}}{(E_\kappa - E_0)^2 + \frac{1}{4}\Gamma_0^2 (E_\kappa / E_0)^4}. \quad (9)$$

Note that for the shape (9), the position of the maximum E_{\max} and the width Γ' do not correspond with the $E_{\max} = E_0$ and $\Gamma' = \Gamma_0$, but it is possible to find limits $E_{\max} \leq E_0$ and $\Gamma' < E_0/2$ for any values of the parameters E_0 and Γ_0 .

As an example, we consider the monopole and dipole resonances. For the 0^+ state, $K_0 = l_x = l_y = 0$ in both T and Y bases, and the cross sections (8) are symmetric for $(\varepsilon_x, \varepsilon_y)$ permutations and are the same for both bases. For 1^- the hypermoment is $K_0 = 1$, and the angular moments (l_x, l_y) can be equal to $(0, 1)$ or $(1, 0)$. Since two neutrons are strongly

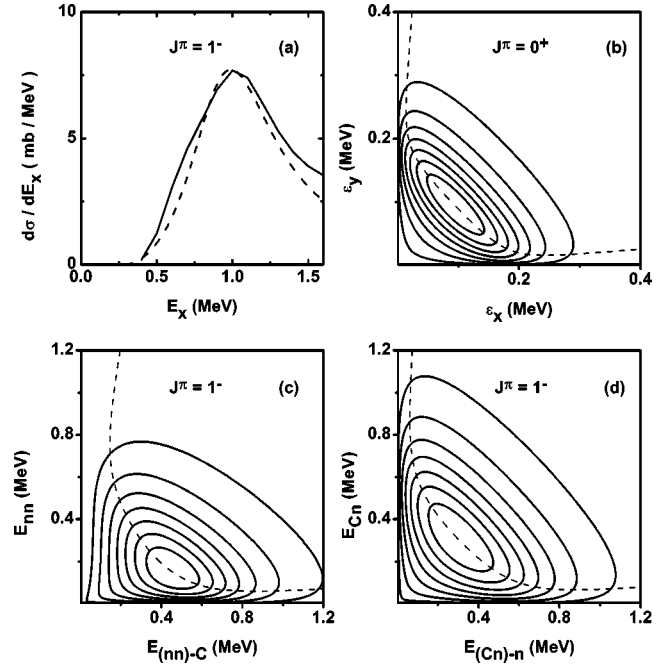


FIG. 3. (a) Solid line shows the theoretical spectrum of the 1^- excitations. Dashed line is the approximation of this spectrum by the three-body resonance from Eq. (9) with parameters $E_0 = 1.2$ MeV and $\Gamma_0 = 4$ MeV. The cross section (8) is calculated for the 0^+ (b) and 1^- [(c) in T and (d) in Y bases] resonances in ^{11}Li . Dashed line shows trajectory of the cross section ridge maxima.

attractive (repulsive) for s -wave (p -wave) motion, the component with $(l_x, l_y) = (0, 1)$ is expected to dominate for dipole excitation in the T basis and gives a cross section which is asymmetric in $(\varepsilon_x, \varepsilon_y)$. In the Y basis this cross section corresponds to motions with angular momenta $(0, 1)$ and $(1, 0)$ with approximately equal weights, and the shape of cross section (8) is close to symmetric.

From Eq. (8) it follows that the contour plot of cross section $\Phi(\varepsilon_x, \varepsilon_y) = d^2\sigma / d\varepsilon_x d\varepsilon_y$ has special patterns for T and Y bases in the $(\varepsilon_x, \varepsilon_y)$ plane in the presence of a “true” three-body resonance. A quantitative tool that can be useful in comparison with real cross sections, is the trajectory of maxima of the cross section “ridge.” This trajectory goes along the curve $\varepsilon_y = \varepsilon_y(\varepsilon_x)$ which is defined by an extremum of the directional derivative of the function $\Phi(\varepsilon_x, \varepsilon_y)$ on the $(\varepsilon_x, \varepsilon_y)$ plane. In the region where the cross section is not small, the trajectory can be well approximated by solving the simpler equation $(d\Phi/d\varepsilon_x)|_{\varepsilon_y = \text{const}} = 0$, obtained by rotation $\pi/4$ of the initial coordinate system: $\varepsilon'_x = 1/\sqrt{2}(\varepsilon_x + \varepsilon_y)$, $\varepsilon'_y = 1/\sqrt{2}(-\varepsilon_x + \varepsilon_y)$.

Figure 3(b) shows the contour plot obtained from Eq. (8) with the parameters $E_0 = 0.25$ MeV and $\Gamma_0 = 0.3$ MeV corresponding to the 0^+ state in ^{11}Li , and the trajectory of the ridge maxima. Figures 3(c) and 3(d) show the contour plots and ridges for the 1^- state in the T and Y bases, respectively. The corresponding spectrum of the three-body resonance from Eq. (9) [dashed line in Fig. 3(a)] is fitted with the model calculations (solid line) described below in Sec. III. An agreement of ridges in real cross sections with the ridges

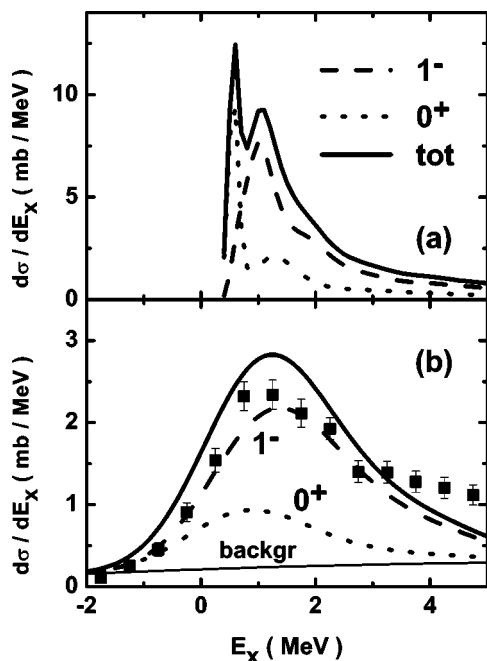


FIG. 4. Excitation energy spectra for ^{11}Li on proton target at collision energy $E/A=68$ MeV. (a) The theoretical spectrum. (b) Comparison of the theoretical spectrum, corrected for experimental conditions, with data measured in experiment [1]. Solid, dashed, and dotted lines show the total, dipole, and monopole cross sections, respectively. In (b), the thin solid line indicates the experimental background from materials other than protons in the target.

in Fig. 3 provides an opportunity to elucidate whether a peak in E_κ is a “true” three-body resonance.

The procedure is clear in the case of a narrow state. A narrow resonance is characterized by a cross section ridge stretched along the straight line $\varepsilon_{\nu_i}=E_0-\varepsilon_{x_i}$. The well known 2^+ resonance in ^6He is the striking example [24].

III. INELASTIC SCATTERING OF ^{11}Li

A. Excitation spectrum of ^{11}Li

Using the nuclear structure model described above and the effective forces checked against the elastic scattering, we can calculate the ^{11}Li inelastic scattering without additional parameters. Figure 4(a) shows the theoretical spectrum $d\sigma/dE_x$ as a function of the ^{11}Li excitation energy measured from the ground state. The spectrum has two peaks near the three-body threshold, corresponding to monopole (dotted line) and dipole (dashed line) transitions.

Figure 4(b) shows a comparison between our calculation and the experimental spectrum measured in Ref. [1] in the $^{11}\text{Li}+p$ collisions at 68 MeV/nucleon. The experimental number of counts given in [1] is here converted to cross sections in mb/MeV. The theoretical curves shown in Fig. 4(b) were obtained from the calculated double differential cross section $d^2\sigma/d\Omega dE_\kappa$ taking into account the experimental acceptance and energy resolution.

Figure 4(b) shows that the experimental data support the calculated accumulation of 0^+ and 1^- transition strength near

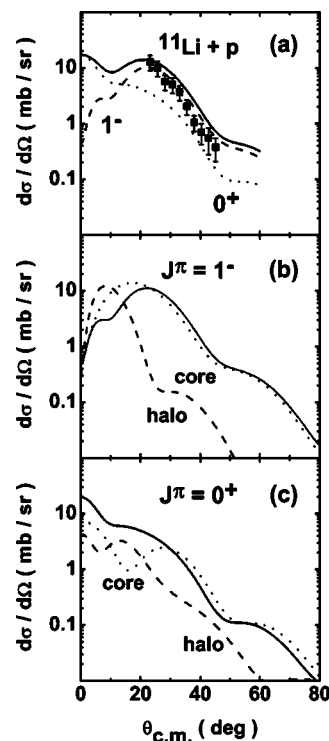


FIG. 5. Angular distributions for the $^{11}\text{Li}+p$ inelastic scattering at $E/A=68$ MeV. (a) Comparison of the theoretical calculations with experimental data [1]. Solid, dashed, and dotted lines show the total, monopole, and dipole angular distributions, respectively. In (b) and (c), solid lines show angular distributions for the monopole and dipole excitations, respectively. Dashed and dotted lines are contributions from the halo neutrons and the core nucleons.

the breakup threshold, even though the fine structure of the theoretical spectrum is washed out by the experimental energy resolution. A reasonable description of both shape and absolute value of the experimental peak is obtained. At higher excitation energies the theoretical calculation underestimates the measured spectrum. It indicates that additional effects, such as ^9Li core excitations and also other multipoles, may have to be included in the model for a better description of the ^{11}Li higher-energy excitations.

B. Inelastic angular distribution

Angular distributions for the $^{11}\text{Li}+p$ inelastic scattering at $E/A=68$ MeV are plotted in Figs. 5(a)–5(c). In Fig. 5(a), the theoretical calculation is compared with the experimental angular distribution [1]. Both shape and absolute value of the calculation are in good agreement with the experimental data. The data include more than one multipole excitation of ^{11}Li , but theory shows that the dipole contribution dominates at large scattering angles, and that experimental data at small angles are needed to reveal the monopole contribution.

The interplay of the core and the halo in the inelastic scattering is illustrated in Figs. 5(b) and 5(c) for dipole and monopole excitations, respectively. Similar to the case of the elastic scattering, the core contributions dominate at large scattering angles. At small angles both contributions are important and the total angular distribution shows strong de-

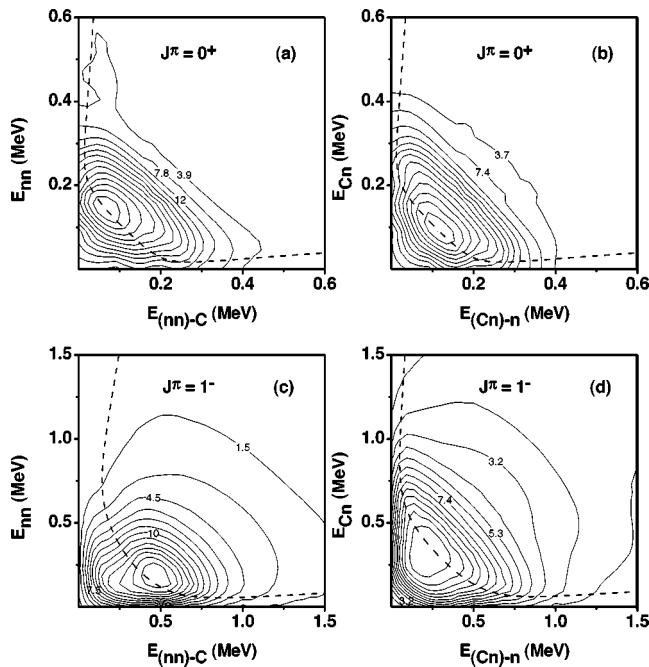


FIG. 6. Theoretical two-dimensional contour plots of ^{11}Li energy correlation cross sections. (a) and (c) show $d^2\sigma/dE_{nn}dE_{(nn)-C}$ for the monopole and dipole excitations, respectively. (b) and (d) show $d^2\sigma/dE_{Cn}dE_{(Cn)-n}$ for the monopole and dipole excitations.

structive (constructive) interference for dipole (monopole) excitations. Reminding results for the elastic scattering, we observe general trend: processes with large momentum transfer are generated by interactions with the core while a cooperation of the halo neutrons and the core characterizes the dynamics at small scattering angles.

In the work of Karataglidis *et al.* [23] the inelastic scattering data of ^{11}Li from protons was calculated using a shakeoff mechanism. The shakeoff approximation reduces all interaction dynamics to the core-target potential, disregarding completely interaction of the target with the halo neutrons. This is approximately true for reaction processes with large transferred momenta, while at small transferred momenta the interactions with all nucleons, halo and core, are equally important and produce a strongly correlated dynamics (see, for example, Figs. 2 and 5). Moreover the interactions with halo neutrons are responsible for the significant increase of the reaction cross section of ^{11}Li compared with ^9Li . Hence we arrive at the conclusion, analogous to the one in Ref. [2], that the shakeoff approximation cannot describe sufficiently accurately the reaction dynamics of halo nuclei.

C. Energy correlations

In addition to the inclusive observables discussed above, we can calculate in our microscopic theory any correlations in these Borromean halo systems, of energy, angular or mixed types. Two-dimensional contour plots of energy correlations are shown in Fig. 6. The monopole and dipole excitations are presented in Figs. 6(a) and 6(c) in T partition, while Figs. 6(b) and 6(d) correspond to the Jacobi coordinates Y .

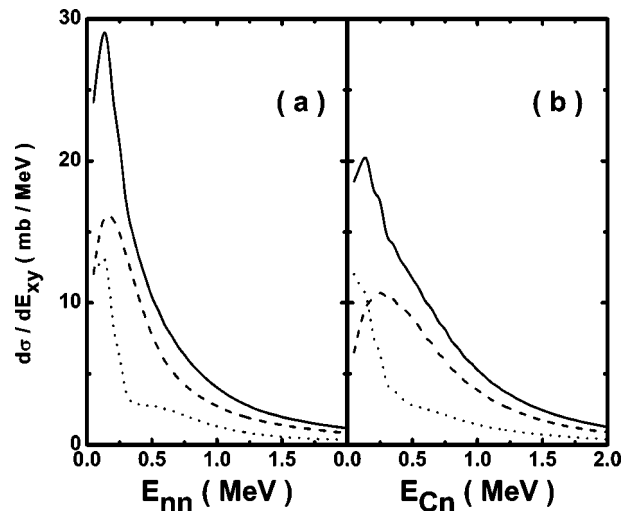


FIG. 7. Theoretical spectra for the relative energy distribution between two halo neutrons (a), and between ^9Li and a halo neutron (b). Dashed and dotted lines show contributions from the dipole and monopole excitations, respectively.

In accordance with Sec. II D, the behavior of the ridge in the cross section in both systems of the Jacobi coordinates provides an opportunity to verify whether a peak over E_{κ} is a “true” three-body resonance. The trajectories of the ridge maxima, which were discussed in Sec. II D and presented in Fig. 3, are again shown by dashed curves in Fig. 6 for our full calculations. In the case of the 0^+ state, Figs. 6(a) and 6(b), the trajectories of the ridge maxima are consistent with each other, indicating a “true” 0^+ three-body resonance. In the 1^- case, this trajectory is in good agreement with the contour plot in Fig. 6(d), while Fig. 6(c) shows deviation. This provides additional indications that 1^- is not a “true” three-body resonance.

Very often, in order to increase statistics, the single differential cross section as a function of some relative energy is extracted from experiments. Such spectra can be obtained by integration of the $d^2\sigma/d\varepsilon_x d\varepsilon_y$ cross sections over ε_x or ε_y . Figure 7 shows examples of such distributions. The relative neutron-neutron and ^9Li -neutron energy spectra, $d\sigma/dE_{nn}$ and $d\sigma/dE_{Cn}$, are given in Figs. 7(a) and 7(b), respectively. The energy distributions fall rapidly and smoothly with increasing energy. Peaks close to the threshold reflect accumulation of transition strength at small energies. The low-energy correlation over E_{nn} can be interpreted as a decay via the singlet n - n state.

D. Angular correlations

Sensitivity to various aspects of reaction dynamics is revealed in the angular correlations shown in Fig. 8.

The cross sections in the Y Jacobi coordinates are shown in Fig. 8(a) as a function of $\cos\theta_{(Cn)-n}$, where $\theta_{(Cn)-n}$ is the angle between the relative (Cn) momentum and the (Cn) - n momentum. The cross sections in the T Jacobi coordinates are shown in Fig. 8(b) as a function of $\cos\theta_{(nn)-C}$, where $\theta_{(nn)-C}$ is the angle between the relative (nn) momentum and the (nn) - C momentum. Dotted and dashed lines show con-

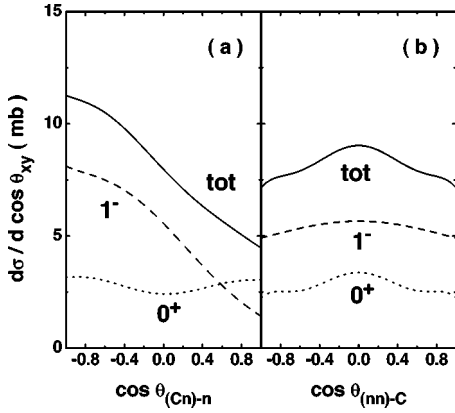


FIG. 8. Angular distributions corresponding to the Y and T sets of Jacobi coordinates, (a) and (b), respectively. Dashed and dotted lines show contributions from the dipole and monopole excitations.

tributions from monopole and dipole excitations, respectively. As a consequence of antisymmetrization between the two halo neutrons, the angular correlation in Fig. 8(b) is symmetric relative to 90° . In contrast, the angular distribution in Fig. 8(a) has a strong asymmetry. Such an asymmetry has previously been measured in a fragmentation of ^{11}Li on carbon target at high energy [25]. The shape of the experimental angular correlation is similar to the calculation in Fig. 8(a). The dipole excitation is responsible for the asymmetry while the monopole excitation creates an isotropic background.

The asymmetrical angular correlation provides evidence concerning mixing of angular momenta with different parities. This follows from the formal expression for the angular correlation [6]

$$\frac{d\sigma}{d \cos \theta_{(Cn)-n}} \propto \sum_{k,\gamma} P_k(\cos \theta_{(Cn)-n}) (l_{Cn} 0 \ l'_{Cn} 0 | k 0) \times (l_{(Cn)-n} 0 \ l'_{(Cn)-n} 0 | k 0) B_\gamma, \quad (10)$$

where l_{Cn} is the orbital angular momentum for relative motion of the $^9\text{Li}-n$ fragments, while $l_{(Cn)-n}$ is the orbital angular momentum for motion of the second neutron relative to the center of mass of the $^9\text{Li}-n$ subsystem. B_γ is a quantity which includes all other factors in the cross section expression which are independent of the angle $\theta_{(Cn)-n}$, and γ is an abbreviation for the quantum numbers that uniquely characterize the motion of the constituents. The asymmetry in the angular correlation arises due to Legendre polynomials $P_k(\cos \theta_{(Cn)-n})$ with odd values of k , $k=1$ being the main term responsible for it. At low excitation energies only low orbital angular momenta, $l_{Cn}, l_{(Cn)-n}=0, 1, \dots$, can have significant weights in the continuum wave functions. To get a large contribution with $k=1$, the motions with orbital momenta $(l_{Cn}, l_{(Cn)-n})=(0, 1)$ and $(1, 0)$ have both to be produced in the reaction with a large probability. Correspondingly, to excite these components in the continuum wave function by the dipole transition, the ground state wave function of ^{11}Li also has to contain s and p waves with comparable and large weights, as is the case of our calculations. The same conclu-

sion on the ^{11}Li ground state structure was also obtained in Ref. [1].

IV. CONCLUSIONS

Inelastic scattering of ^{11}Li on a proton target at collision energy of 68 Mev/nucleon [1] has been analyzed in the framework of the microscopic four-body distorted-wave model [4,6]. The ground state and the three-body continuum excitations of ^{11}Li were calculated in the three-body $^9\text{Li}+n+n$ cluster model [9] using the method of hyperspherical harmonics [11]. Effective density-dependent nucleon-nucleon forces have been used for the interaction of the proton target with the core nucleons, while free t -matrix forces were used for interaction with the halo neutrons. The parameters of the effective forces were checked by calculating the single folding optical potentials which were applied to description of experimental data on the elastic scattering of both ^9Li and ^{11}Li on proton. The theory describes well the available elastic scattering data and correctly reproduces the experimentally observed difference in cross sections for ^{11}Li and ^9Li . This difference is explained by a motion of the ^9Li core within ^{11}Li . Thus there are no new parameters when the theory is applied to inelastic scattering of ^{11}Li .

The calculations of inelastic scattering show accumulation of dipole and monopole excitations of ^{11}Li near the three-body threshold and describe well the observed peak in the experimental energy spectrum of ^{11}Li . Also, the theory reproduces well the corresponding experimental angular distribution and confirms a dominance of the dipole excitation. To reveal clearly the monopole excitation, experimental data at small angles are needed.

Concerning the reaction dynamics, a proper treatment of translational invariance is vitally important for halo nuclei. Reaction processes with large transferred momenta are mainly defined by interactions with the core nucleons, while at small transferred momenta the interactions with all nucleons, core and halo, are equally important and produce a strongly correlated dynamics.

Investigations of a variety of angular and energy correlations between constituents are necessary to explore in detail the nature of halo nuclei. Various correlations are sensitive to different aspects of reaction mechanism and nuclear structure. To unravel the nature of halo excitations and establish their character, two-dimensional plots of energy correlations of fragments were shown to be useful. We investigated ridges in the calculated two-dimensional energy plots for ^{11}Li and obtained an indication, that while the monopole excitation is a “true” three-body resonance, a deviating behavior of the cross section ridge in the case of the dipole excitation provides new and additional evidence that it is not a “true” three-body resonance. This supports results of Ref. [2] based on phase shift analysis. Furthermore, angular correlations are sensitive to the partial orbital composition of halo excitations. Our calculations of angular correlations in the ^{11}Li inelastic scattering show that a mixture of angular momenta with different parities in the $^9\text{Li}+n+n$ continuum leads to asymmetry in the case of the dipole excitation.

Thus, simultaneous analysis of a variety of observables

within the same theory is used to reduce ambiguities of model assumptions related to the reaction dynamics. We have shown that correlations in breakup reactions can be a viable tool for exploring the genuine nature of halo continua. Kinematically complete experiments under conditions where a one-step reaction mechanism dominates are most promising and reliable instruments for investigations of halo structure.

ACKNOWLEDGMENTS

The authors thank M. V. Zhukov for fruitful discussions. Two of the authors (S.E. and B.D.) are thankful to the University of Bergen for hospitality and acknowledge support from RFBR Grants No. 02-02-16174 and No. 1885.2003.2. S.E., B.D., and I.T. acknowledge support from EPSRC Grants No. GR/R25514 and No. G/M82141.

-
- [1] A. A. Korshennikov *et al.*, Phys. Rev. Lett. **78**, 2317 (1997).
 [2] R. Crespo, I. J. Thompson, and A. A. Korshennikov, Phys. Rev. C **66**, 021002(R) (2002).
 [3] S. N. Ershov *et al.*, Phys. Rev. C **56**, 1483 (1997).
 [4] S. N. Ershov, B. V. Danilin, T. Rogde, and J. S. Vaagen, Phys. Rev. Lett. **82**, 908 (1999).
 [5] S. N. Ershov, B. V. Danilin, and J. S. Vaagen, Phys. Rev. C **62**, 041001(R) (2000).
 [6] S. N. Ershov, B. V. Danilin, and J. S. Vaagen, Phys. Rev. C **64**, 064609 (2001).
 [7] B. V. Danilin *et al.*, Phys. Rev. C **43**, 2835 (1991).
 [8] I. Tanihata *et al.*, Phys. Rev. Lett. **55**, 2676 (1985).
 [9] M. V. Zhukov *et al.*, Phys. Rep. **231**, 151 (1993).
 [10] B. V. Danilin, I. J. Thompson, M. V. Zhukov, and J. S. Vaagen, Nucl. Phys. **A632**, 383 (1998).
 [11] B. V. Danilin and M. V. Zhukov, Yad. Fiz. **56**, 67 (1993) [Phys. At. Nucl. **56**, 460 (1993)].
 [12] D. Gogny, P. Pires, and R. de Tournell, Phys. Lett. **32B**, 591 (1970).
 [13] I. J. Thompson and M. V. Zhukov, Phys. Rev. C **49**, 1904 (1994).
 [14] I. J. Thompson *et al.*, J. Phys. G **24**, 1505 (1998).
 [15] J.-P. Jeukenne, A. Lejeune, and C. Mahaux, Phys. Rev. C **16**, 80 (1977).
 [16] G. Bertsch, J. Borysowicz, H. McManus, and W. G. Love, Nucl. Phys. **A284**, 399 (1977).
 [17] F. Petrovich *et al.*, Nucl. Phys. **A563**, 387 (1993).
 [18] M. A. Franey and W. G. Love, Phys. Rev. C **31**, 488 (1985).
 [19] C.-B. Moor *et al.*, Phys. Lett. B **297**, 39 (1992).
 [20] A. A. Korshennikov *et al.*, Nucl. Phys. **A617**, 45 (1997).
 [21] N. B. Shul'gina and B. V. Danilin, Nucl. Phys. **A554**, 137 (1993).
 [22] B. V. Danilin, T. Rogde, J. S. Vaagen, I. J. Thompson, and M. V. Zhukov, Phys. Rev. C **69**, 024609 (2004).
 [23] S. Karataglidis, P. G. Hansen, B. A. Brown, K. Amos, and P. J. Dortmans, Phys. Rev. Lett. **79**, 1447 (1997).
 [24] B. V. Danilin, J. S. Vaagen, I. J. Thompson, and M. V. Zhukov, Few-Body Syst., Suppl. **13**, 122 (2001).
 [25] H. Simon *et al.*, Phys. Rev. Lett. **83**, 496 (1999).